Edge versus interior in the chemical bonding of graphene materials

Michael R. Philpott* and Yoshiyuki Kawazoe
Institute for Materials Research, Tohoku University, Aoba-ku, Sendai 980-8577, Japan
(Received 9 May 2009; published 8 June 2009)

A notable phenomenon is described involving the polarization of valence electrons that operates in the edge regions of graphene materials, including compact polyaromatic hydrocarbon (PAH) molecules, because of the mismatch between interior and perimeter chemical bonds. The topology of hexagonal-shaped zigzag-edged systems, with alternating perimeter CC bond lengths, enhances the effect, making recognition easier, compared to graphene ribbons where it is weak. The phenomenon is delineated in *ab initio* density-functional theory calculations of the electronic structure of a 4 nm diameter hexagonal zigzag-edged molecule $C_{486}H_{54}$, chosen because it is a representative of larger ones. Using CC bond length as a surrogate measure, we map the polarization of valence electrons from the perimeter to the center. In a pattern that mimics the bonding, the polarization of the two outermost sets of edge bonds (transverse along rows and radial connecting nested rows of carbon atoms) is impressed on the graphene interior bonds with amplitude that decreases rapidly from the perimeter to the center. All bonds display a decaying oscillation with radial bonds longer than transverse bonds at the same location. This difference leads to a characteristic quinoidal pattern of CC bonds linking the zigzag hexagonal edges joined at each apex. The phenomenon and its analysis are applicable to geometries periodic or not, substituent modified edges and interior.

DOI: 10.1103/PhysRevB.79.233303 PACS number(s): 73.22.−f, 61.46.Df, 62.23.Eg, 71.15.−m

Graphene sheets and large compact polyaromatic hydrocarbon (PAH) molecules offer the possibility of manufacturable nanoscale electronic devices and even computers on molecules. Three events have fueled these developments. Berger *et al.*[1] demonstrated epitaxial growth of graphene monolayers and multilayers on silicon carbide. Novoselov *et al.*[2] peeled micron-sized graphene sheets from graphite crystals. Wu *et al.*[3] synthesized the large hexagonal molecule $C_{222}H_{42}$, demonstrating how the gap between molecules and flakes can be bridged from the small side. Exploitation of graphene materials for nanoelectronic applications requires a deep understanding of how edge topology impacts the geometric and electronic structures. In two dimensions (2D) there is no screening of long-range interactions and whereas the sigma CC bonding network is highly localized, the pi-bonding system is not so constrained. Witness the ability of the pi systems to couple spins on adjacent and distant edges.[4–7] There has been much less effort in understanding the geometry.

We demonstrate an unusual effect, whereby the pi system of the edge atoms impresses on the interior, row by row, an electronic polarization characteristic of the edge topology. This polarization decays rapidly with distance from the perimeter into the interior so that after about four rows the latter has the properties of infinite graphene. Though the phenomenon is quite general, it is most clearly seen in large hexagonal-shaped graphene molecules with zigzag edges. Accordingly we examine one of these systems in detail and delay until later comment on general systems and the underlying physics.

We have determined the electronic and geometric structures of the singlet antiferromagnetic spin ground state, singlet spin paired, and lowest triplet state of $C_{486}H_{54}$, the $m=9$ member of a series of hexagonal-shaped PAHs with zigzag edges and general formula $C_{6m**2}H_{6m}$ $(m=2,\ldots,10)$. The geometries are all very similar, so we use only the singlet spin paired data in the figures. Based on trends along the entire series, the molecule $C_{486}H_{54}$ has a graphene central zone, an established perimeter and is the first in the series to have a singlet ground state with an antiferromagnetic spin distribution on a hexagonally sectored bipartite lattice. The model for the interior is an infinite graphene. A suitable model for the perimeter does not exist. Useful comparisons are planar D_{6h} annulene $C_{102}H_{102}$ that has almost uniform CC bonding along the chain and the linear D_{2h} acene nonacene $C_{38}H_{22}$ that has decreasing bond alternation from each end, tending to uniform bonding in the middle of the molecule.

The calculations used *ab initio* plane-wave-based density-functional theory (DFT) methodology, with projector augmented wave potentials[8–10] and the spin polarized generalized gradient approximation with the exchange-correlation energy functional parametrized by Perdew *et al.*[11] All valence electrons were included. The plane-wave energy cutoff was 400 eV. Calculations were done in a periodic tetragonal cell with $6.0\times6.0\times1.5$ nm^3 edges. Atoms in different cells were more than 1.5 nm apart. Brillouin-zone integrations were done at the gamma point. Geometry optimization was done with atoms constrained to a plane until forces acting on any ion were less than 3.4 μeV/pm. Room-temperature graphite has $a=245.6$ pm and CC=141.8 pm. Our calculations of periodic graphene yielded $a=246.7$ pm and bond CC=142.4 pm. These, similar to the previous ones,[12] slightly exceed the experimental values.

Prior calculations showed that in PAHs the CC bond length is directly proportional to the maximum isometric surface charge (MISC) density on the stick bond joining carbon atoms.[13] In a new set including acetylene, ethylene, ethane, benzene, pyrene, and coronene, a plot MISC vs CC length was almost linear in the range 120–153 pm. Using the CC bond length as a surrogate measure, we analyzed the isometric surfaces of the total valence charge density and obtained a description of the two zones, interior and perimeter, their separation by long radial CC bonds and the polarization of the interior valence charge patterned after the topology of the outermost set of transverse and radial bonds (notation: trans-

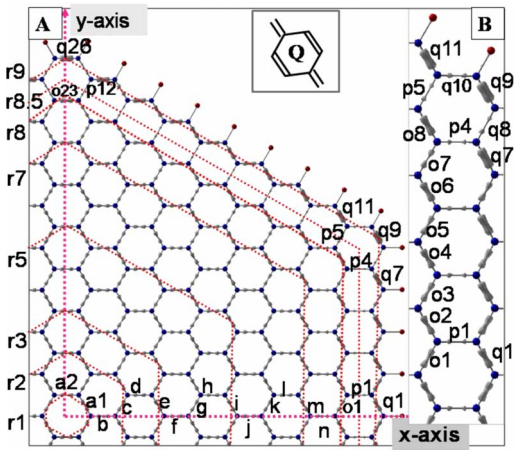

FIG. 1. (Color online) The main panel A shows a converged geometry of the (+,+) quadrant of molecule $C_{486}H_{54}$ with stick bonds and an overlay of an isometric surface of the total charge density (ρ=2.02e/Å^3), together with the labeling of CC bonds used in text. Labels r1, r2,…, r9 on the left side indicate some of the nested hexagonal rows of carbon atoms. Panel B is a detail of the right side vertical edge. Inset panel Q shows an idealized quinoid ring in standard organic notation.

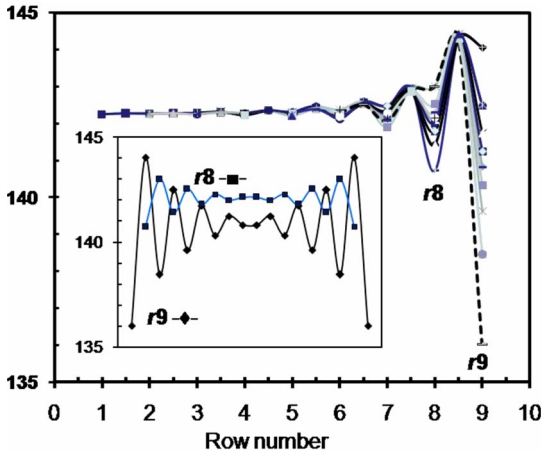

FIG. 2. (Color online) Plots of bond length (/pm) vs row label for all CC bonds in the (+,+) quadrant of the molecule. The coordinate is the row number, integers (1, 2,…, 9) for the transverse and half odd integers (1.5, 2.5,…, 8.5) for the radial bonds. The inset panel shows the variation in length of transverse bonds along rows r9 and r8.

verse bonds connect atoms along rows and radial bonds connect nested rows of carbon atoms).

Figure 1, main panel A, shows for the (+,+) quadrant of the $C_{486}H_{54}$ molecule an isometric surface of the total charge density (singlet spin paired state) overlaid on the optimized geometry with atoms connected by stick bonds. The dotted lines denote some (not all) of the nested set of nine hexagonal rows of carbon atoms, labeled r1, r2,…, r9 on the left-hand side (LHS) of the figure. The alphabetical labeling of CC bonds, shown along the x axis, starts from the molecular center. The bonds have numerical labels for D_{2h} symmetry as would be appropriate for a triplet S=1 state. All bonds, transverse and radial, are arrayed in nested hexagonally rows. We label the hexagonal rows of bonds alphabetically (a, b, c,…, q) from the center and the individual bonds along each row numerically, 1, 2, 3,…, in a counterclockwise rotation starting from the x axis. The bonds are either transverse (a, c, e,…, q), meaning they join atoms in the same zigzag row with integer labels, or radial (b, d, f,…, p), meaning they join atoms in adjacent rows. The hexagonal rows of radial bonds are assigned a half odd integer value r1.5, r2.5, r3.5,…, r8.5. In referencing bonds we occasional use the hybrid notation r3.5(f3) which specifies the CC bond f3 in row r3.5.

Next we re-examine the charge density displayed in Fig. 1 panel A and the edge detail in panel B. The enlarged view in panel B shows the isometric surface more clearly. The isometric surface charge density (ρ=2.02e/Å^3) was selected high so that most of the radial bonds r8.5(p1,…, p12), joining the penultimate row r8 to the perimeter row r9 atoms, appear as bare sticks because they have no charge density higher than the chosen value. Visible in the apex is the shortest bond q9 which has the largest isometric surface. This bond is part of a quinoidal structure (see chemical bonding in panel Q). In panel A the bonds q7, q9, q11, and o8 (o8 is not labeled) belong to a quinoidal pattern of four short (transverse) bonds linked by four longer radial bonds q8 (not labeled), p4, p5, and q10 (not labeled). In panel B following the perimeter bonds along (down) the edge from q9 to q1, we see the initial strong alternation in charge fading to a more uniform shape at the center of the edge.

Figure 2 shows a plot of bond length vs row label for all the bonds in the (+,+) quadrant of the molecule. The coordinate is the row number, an integer (1, 2,…, 9) for the transverse bonds on each nested row of carbon atoms and a half integer (1.5, 2.5,…, 8.5) for the radial bonds that join the nested rows. The curves (drawn to assist the eye) trace back from the perimeter to the smallest row from which a transverse and radial bond start in the labeling scheme in Fig. 1, so radial and transverse bonds can belong to the same curve. The bonds oscillate in length with the radial bonds as a group being longer than the transverse bonds on either side. This unusual result has been warranted in calculations using finer grids and a larger plane-wave energy cutoff. In this hexagonal system there are half as many radial compared to transverse bonds, so a two-dimensional isotropic decompression originating from the edge of the molecule would lengthen radial bonds relative to the transverse. In the center of the molecule the oscillation is very small, all bond lengths are essentially the same, and the graphene zone extends out to row 6, that is, to within four rows from the perimeter. This is an important result having obvious implications for the modeling of the chemical reactions of graphene edges using small molecules. Since all the bonds are plotted in Fig. 2, the differences along each row show as a dispersion of the curves at each row index. The dispersion in transverse bond lengths increases greatly beyond row 6 ending with the largest range on the perimeter. In Fig. 2 the inset panel shows the variation in the transverse bond lengths on rows r9 and r8 plotted along one side of the hexagonal molecule. The curves are centered symmetrically on the middle of the row, showing that row r8 has two bonds less than the perimeter set. With few exceptions transverse bonds get shorter as their row approaches the perimeter.

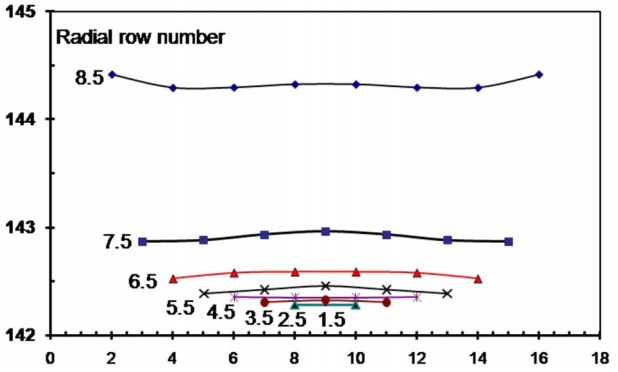

FIG. 3. (Color online) Variation in the length (/pm) of radial CC bonds vs position relative to the center of each row. There is one curve per row. The row numbers are shown as the half integer labels on the LHS of each curve. The data points are interdigitated, consistent with their spatial position in the molecule shown in Fig. 1.

Radial bonds have a different trend, they exhibit little dispersion within their row, and all jump in length as the perimeter is approached. The radial bonds in the row 8.5 are the longest in the molecule. Radial bond variations along each row ($n.5$ with $n=1,2,\ldots,8$) are shown in Fig. 3. The row numbers are shown as half integer labels on the LHS of each curve. The curves show that there is little variation along a given row. The coordinate denotes the position along the row. In the direction of the center of the molecule, succeeding rows have one bond less. Accordingly in Fig. 3 each curve is centered on coordinate axis position 9, presenting an interdigitate set of points consistent with their spatial position in the molecule (see Fig. 1). The central point in the lowest curve marks the radial bond r1.5(b) on row r1.5 in Fig. 1. The curves have the property of being shape similar, meaning their shape is independent of the number of data points. The radial bonds, mostly constant within the row, decrease the most between the r8.5 and r7.5. Thereafter they converge quickly to the central value. This change in bond length with row can be fitted to a polynomial function. The near constancy of the radial bonds on a particular row is an important feature that provides the long bond sides of the quinoidal structures present within the real estate of each apex.

Figure 4 shows smooth curves drawn through data points for transverse bonds on each row from row r9 (perimeter) to row r1 (center). Note that in the middle of each row the transverse bonds converge from below on the bond length of the central row r1. This is opposite to the radial bonds, which converge from above and contributory factor to the bond-length oscillation seen in Fig. 2. Consider the transverse bonds of the perimeter row. In Fig. 1 these have the labels r9(q1) (mid row) to r9(q9) (apex) to r9(q26) (apex). Starting from the apex (Fig. 1, q9 or q26, CC $\sim$ 136 pm), the bonds display a decreasing alternation toward a more uniform value in the middle of the edge, where CC $\sim$ 141 pm. Although the main panel shows all the curves, only the easily distinguished ones in rows r9, r8, r7, and r1 are labeled. Curves for rows r6, r5, and r4 are shown separately in the middle set and curves for rows r3, r2, and r1 in the bottom set. The middle and lower data sets are shown displaced downward and have

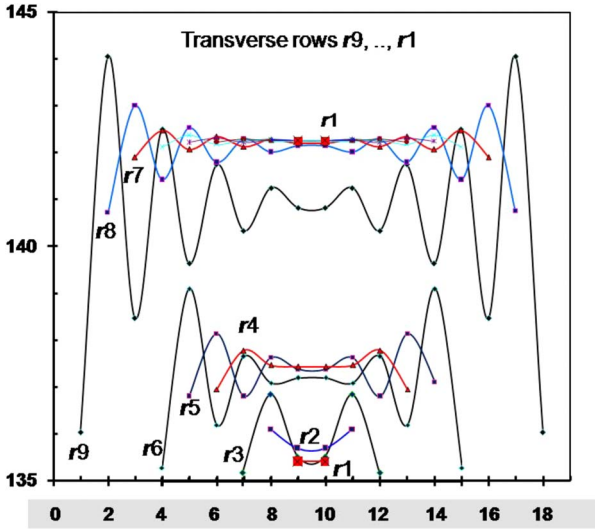

FIG. 4. (Color online) Variation in the length (/pm) of transverse bonds along rows r9 (perimeter) to r1 (center). All the curves for the transverse bonds have a self-similar shape. Rows r9, r8, r7, and the central row r1 are labeled in the main panel. The inset panels separately show the bonds for rows r6, r5, r4 and rows r3, r2, r1 on expanded (vertical) and shifted length scales at the same (horizontal) position as in the main panel.

greatly expanded bond-length scales. The set of curves for the transverse bonds have a self-similar shape in the sense that each succeeding curve resembles the next longest row with the row end oscillations removed. Taken together these radial and transverse bond variations permit a detailed look at the range and distance dependence of the interior-perimeter interaction. Starting from the shortest bonds the curves serve to focus attention on the strong bond alternation along the perimeter. Their pattern, with the large apex oscillation and more uniform midedge value, resembles that found for the linear acene nonacene $C_{38}H_{22}$ except for an offset due to the two cross-linking bonds at each end of the acene molecule.

The mechanism causing the polarization can be understood using the ideas underlying the Koster-Slater theory of impurity levels[14] applied to edges. The difference between perimeter and interior atoms provides an interaction which localizes levels at the top of the valence band. The charge density of this collection of highest occupied molecular orbital (HOMO) levels is spread in a decaying fashion onto the neighboring interior rows, causing bond lengths to change. The topology of the perimeter controls the polarization pattern and which part of an interior row is most affected. Partial charge densities of the Kohn-Sham levels verify the localization and range of the polarization. By analogy with the Rashba effect[15] in doped molecular crystals, other phenomena of a collective or cooperative nature may be manifested in graphenes.

The geometry of the representative hexagonal zigzag-edged molecule $C_{486}H_{54}$ is the result of competing effects, the central region strives to adopt the geometry of infinite graphene and the zigzag perimeter in isolation strives for a uniformly conjugated geometry permitting pi-electron delocalization. The interaction between the interior and perimeter

results in CC bonds joining perimeter row (r9) to the penultimate row (r8.5) getting long (but well short of single CC =153 pm), facilitating some separation of perimeter from the interior. This elongation acts to reduce the polarizing interaction of the perimeter across the radial row r8.5 bonds. The net result is an imprinting from the edge onto the interior of an electronic polarization which is manifest as self-similar bond variations in the interior rows. In a hexagonal-shaped zigzag system a direct consequence of these interactions is the appearance of a pattern of linked quinoidal C_6 rings extending out on either side of each apex.

For periodic zigzag-edged graphene strips the phenomenon is weak, present mostly in the radial bonds because bonds with a projection on the periodic direction are constrained. Figure 5 shows the dependence of the CC bond length (pm) for a simple zigzag nanoribbon that is 15 rings wide (y axis) and one ring periodic along the x direction. The periodic cell formula was $C_{32}H_2$. The change in transverse bonds is about half or less of the radial bonds, and deviations from the ribbon center occur only near the perimeter. Unit-cell periodic width was set to the graphene distance corresponding to CC=142.4 pm. In the nanoribbons the occurrence of edge states localized in the density of states near the Fermi level was recognized early on,[16] but not the general nature of the phenomenon as described here.

In large crenelated (arm chair) edged graphene molecules the MISC polarization effect was observed[17] within the apex region as a regular C_6 ring with six equilength radiating CC bonds that are longer than the ring bond. This particular pattern is characteristic of the aromatic sextet of the so-called fully benzenoid aromatic hydrocarbons.[18] It occurs across small crenelated hexagonal PAH but as they get larger the interior pattern fades leaving only vestiges in the apex regions.[17] Edges with triangular protrusions also have distinctive patterns.[13]

These results for the apexes of finite-sized molecules can be generalized to periodic systems with protrusions, defects, substituted, or derivatized edges and interior. In graphene systems with ragged edges, defects, or substituents, there will be a polarization distortion from the affected region impressed on the interior bonds or surroundings. Its form will be characteristic of the electronic and geometric structures of the irregularity. Available scanning tunnel microscope (STM) images of ragged graphene edges already hint at some of these effects.[19] Complex even rough geometries can be analyzed using the basic ideas presented here. The design of graphene devices and study of graphene growth and combustion[20] will benefit from the understanding of edge vs interior provided by this Brief Report.

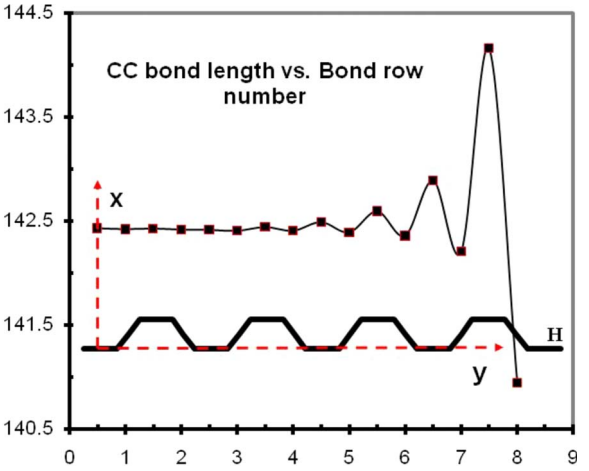

FIG. 5. (Color online) Variation in CC bond lengths (/pm) in a simple zigzag nanoribbon that is 15 rings wide along the y axis and periodic in one ring along the x axis. Row 8 is the zigzag perimeter of transverse CC bonds and row 0.5 is the location of the row of central radial bonds. The unit-cell formula is $C_{32}H_2$. The bonding in one half of the unit cell is shown schematically as stick bonds drawn along the y axis. The radial bonds are longer than the transverse bonds at the same location. The perimeter-interior polarization phenomenon is relatively weak in this system compared to the hexagonal zigzag ones.

All calculations were performed on the IMR SR11000 Super Computer. The facility staff are thanked for their dedicated support. M.R.P. thanks the JSPS organization for research support.

*Corresponding author; philpott@imr.edu

[1] C. Berger *et al.*, J. Phys. Chem. B **108**, 19912 (2004).
[2] K. S. Novoselov *et al.*, Proc. Natl. Acad. Sci. U.S.A. **102**, 10451 (2005).
[3] J. Wu *et al.*, Chem. Rev. (Washington, D.C.) **107**, 718 (2007).
[4] S. Okada and A. Oshiyama, Phys. Rev. Lett. **87**, 146803 (2001).
[5] J. Fernandez-Rossier and J. J. Palacios, Phys. Rev. Lett. **99**, 177204 (2007).
[6] W. L. Wang *et al.*, Nano Lett. **8**, 241 (2008).
[7] D.-E. Jiang *et al.*, J. Chem. Phys. **127**, 124703 (2007).
[8] G. Kresse and J. Hafner, Phys. Rev. B **47**, 558 (1993); **49**, 14251 (1994).
[9] G. Kresse and J. Furthmüller, Comput. Mater. Sci. **6**, 15 (1996); Phys. Rev. B **54**, 11169 (1996).
[10] P. E. Blöchl, Phys. Rev. B **50**, 17953 (1994); G. Kresse and D. Joubert, *ibid.* **59**, 1758 (1999).
[11] J. P. Perdew and Y. Wang, Phys. Rev. B **45**, 13244 (1992); J. P. Perdew, in *Unified Theory of Exchange and Correlation Beyond the Local Density Approximation in Electronic Structure of Solids 1991*, edited by P. Ziesche and H. Eschrig (Akademie-Verlag, Berlin, 1991).
[12] M. Itoh *et al.*, Phys. Rev. Lett. **102**, 055703 (2009).
[13] M. R. Philpott *et al.*, Mater. Trans. **49**, 2448 (2008); Chem. Phys. **354**, 1 (2008).
[14] G. F. Koster and J. C. Slater, Phys. Rev. **95**, 1167 (1954).
[15] E. I. Rashba, Opt. Spektrosk. **2**, 568 (1957).
[16] K. Nakada *et al.*, Phys. Rev. B **54**, 17954 (1996); M. Fujita *et al.*, J. Phys. Soc. Jpn. **65**, 1920 (1996).
[17] M. R. Philpott and Y. Kawazoe, Chem. Phys. **358**, 85 (2009).
[18] E. Clar, *Polycyclic Hydrocarbons*, (Academic, London 1964); *The Aromatic Sextet* (Wiley, New York, 1972).
[19] Y. Kobayashi *et al.*, Phys. Rev. B **73**, 125415 (2006).
[20] R. Whitesides *et al.*, Proc. Combust. Inst. **31**, 539 (2007).